

Article

## Synthesis of Uniform Disk-Shaped Copper Telluride Nanocrystals and Cation Exchange to Cadmium Telluride Quantum Disks with Stable Red Emission

Hongbo Li, Rosaria Brescia, Mauro Povia, Mirko Prato, Giovanni Bertoni, Liberato Manna, and Iwan Moreels

*J. Am. Chem. Soc.*, **Just Accepted Manuscript** • DOI: 10.1021/ja404694k • Publication Date (Web): 18 Jul 2013

Downloaded from <http://pubs.acs.org> on July 19, 2013

### Just Accepted

“Just Accepted” manuscripts have been peer-reviewed and accepted for publication. They are posted online prior to technical editing, formatting for publication and author proofing. The American Chemical Society provides “Just Accepted” as a free service to the research community to expedite the dissemination of scientific material as soon as possible after acceptance. “Just Accepted” manuscripts appear in full in PDF format accompanied by an HTML abstract. “Just Accepted” manuscripts have been fully peer reviewed, but should not be considered the official version of record. They are accessible to all readers and citable by the Digital Object Identifier (DOI®). “Just Accepted” is an optional service offered to authors. Therefore, the “Just Accepted” Web site may not include all articles that will be published in the journal. After a manuscript is technically edited and formatted, it will be removed from the “Just Accepted” Web site and published as an ASAP article. Note that technical editing may introduce minor changes to the manuscript text and/or graphics which could affect content, and all legal disclaimers and ethical guidelines that apply to the journal pertain. ACS cannot be held responsible for errors or consequences arising from the use of information contained in these “Just Accepted” manuscripts.



1  
2  
3  
4  
5  
6  
7  
8  
9  
10  
11  
12  
13  
14  
15  
16  
17  
18  
19  
20  
21  
22  
23  
24  
25  
26  
27  
28  
29  
30  
31  
32  
33  
34  
35  
36  
37  
38  
39  
40  
41  
42  
43  
44  
45  
46  
47  
48  
49  
50  
51  
52  
53  
54  
55  
56  
57  
58  
59  
60

# Synthesis of Uniform Disk-Shaped Copper Telluride Nanocrystals and Cation Exchange to Cadmium Telluride Quantum Disks with Stable Red Emission

*Hongbo Li<sup>1,#</sup>, Rosaria Brescia<sup>1,#</sup>, Mauro Povia<sup>1</sup>, Mirko Prato<sup>1</sup>, Giovanni Bertoni<sup>1,2</sup>, Liberato Manna<sup>1</sup> and Iwan Moreels<sup>1,\*</sup>*

<sup>1</sup> *Istituto Italiano di Tecnologia, via Morego 30, IT-16163 Genova, Italy.*

<sup>2</sup> *IMEM-CNR, Parco Area delle Scienze 37/A, IT-43124 Parma, Italy.*

\* [iwan.moreels@iit.it](mailto:iwan.moreels@iit.it)

# contributed equally to this work.

KEYWORDS copper telluride, cadmium telluride, quantum dots, shape control, cation exchange, photoluminescence

1  
2  
3 ABSTRACT  
4  
5  
6

7 We present the synthesis of novel disk-shaped hexagonal  $\text{Cu}_2\text{Te}$  nanocrystals with a well-defined  
8 stoichiometric composition, and tunable diameter and thickness. Subsequent cation exchange of  
9 Cu to Cd at high temperature (180 °C) results in highly fluorescent CdTe nanocrystals, with less  
10 than 1 mol.% of residual Cu remaining in the lattice. The procedure preserves the overall disk  
11 shape, but is accompanied by a substantial reconstruction of the anion sublattice, resulting in a  
12 reorientation of the  $c$ -axis from the surface normal in  $\text{Cu}_2\text{Te}$  into the disk plane in CdTe  
13 nanodisks. The synthesized CdTe nanodisks show a continuously tunable photoluminescence  
14 (PL) peak position, scaling with the thickness of the disks. The PL lifetime further confirms that  
15 the CdTe PL arises from band-edge exciton recombination, *i.e.* no Cu-related emission is  
16 observed. On average, the recombination rate is about 25-45% faster with respect to their  
17 spherical quantum dots counterparts, opening up the possibility to enhance the emission rate at a  
18 given wavelength by controlling the nanocrystal shape. Finally, with a PL quantum efficiency of  
19 up to 36% and an enhanced PL stability under ambient conditions due to a monolayer of CdS  
20 formed on the nanocrystal surface during cation exchange, these flat quantum disks form an  
21 interesting enrichment to the current family of highly fluorescent, shape-controlled nanocrystals.  
22  
23  
24  
25  
26  
27  
28  
29  
30  
31  
32  
33  
34  
35  
36  
37  
38  
39  
40  
41  
42  
43  
44  
45  
46  
47  
48  
49  
50  
51  
52  
53  
54  
55  
56  
57  
58  
59  
60

## Introduction

In recent years, we have seen a remarkable progress in the size- and shape-control of colloidal nanocrystals. Next to spherical core and core/shell quantum dots,<sup>1,2</sup> the synthesis of nanowires and nanorods is already well established,<sup>3-5</sup> and by now several protocols also allow extending their shape to flat nanodisks and larger 2D nanosheets.<sup>6,7</sup> Recent developments have also produced flat core/shell nanocrystals, *e.g.* CdSe/CdS nanocrystals with a dot-in-disk motive yielding an emission strongly polarized in two dimensions,<sup>8</sup> or 2D CdSe nanosheets passivated with a thin layer of CdS via solution atomic layer deposition.<sup>9</sup>

Compared to the synthesis of quantum dots and rods, for several materials it is still challenging to prepare fluorescent quantum disks, *i.e.* 0D quantum confined flat or highly oblate nanocrystals. Indeed, while this shape is easily obtained in copper sulfide and selenide nanocrystals,<sup>10-12</sup> for II-VI, IV-VI, or other chalcogenide materials only larger 2D sheets are grown, either by exfoliation of thin films or oriented attachment of small clusters, in both cases leaving little control over the lateral dimensions.<sup>6,13-15</sup> Yet from both a structural and optical perspective, nanodisks may show advantages over extended sheets: we can expect an improved control over their assembly into superlattices,<sup>16</sup> and a continuous tunability of their band-edge absorption and photoluminescence (PL) by varying the dimensions of the disk. To this end, the control over all spatial dimensions of the nanodisk is of course crucial.<sup>13,17</sup>

For nanocrystal compositions and shapes that are difficult to grow by direct synthesis approaches, cation exchange reactions have emerged as an extremely useful alternative route.<sup>18-20</sup> Recently copper chalcogenides were recognized as a high quality template for cation exchange.<sup>21,22</sup> Furthermore, as in this material class several disk-shaped nanocrystals are already

1  
2  
3 reported in literature,<sup>10,23</sup> we can take full advantage of both features. In this manuscript, we will  
4  
5 first present the synthesis of novel Cu<sub>2</sub>Te copper telluride nanodisks with controlled thickness  
6  
7 and diameter, as protocols are far less developed compared to copper sulfide and selenide  
8  
9 nanocrystals.<sup>24-26</sup> Next, we perform a cation exchange reaction to obtain highly fluorescent CdTe  
10  
11 quantum disks, paying particular attention to the preservation of the overall shape. As a result of  
12  
13 the hexagonal crystal structure of the initial Cu<sub>2</sub>Te disks, we obtained wurtzite CdTe quantum  
14  
15 disks. This is a metastable phase at room temperature for bulk CdTe, therefore the resulting opto-  
16  
17 electronic properties of the quantum disks may be of particular interest. The passivation of the  
18  
19 surface with sulfur atoms, due to the thiol ligands used in the copper telluride synthesis, and the  
20  
21 conservation of this layer in the following cation exchange reaction leads to an enhanced PL  
22  
23 stability of the CdTe quantum disks compared to spherical CdTe quantum dots prepared by a  
24  
25 conventional approach. The PL quantum efficiency was as high as 36%, and we observed a  
26  
27 faster PL decay rate compared to the quantum dots, which we could attribute (in part) to a  
28  
29 reduced average dielectric screening induced by the peculiar shape of the disks.  
30  
31  
32  
33  
34  
35  
36  
37  
38  
39

## 40 **Experimental**

41  
42 **Materials.** Cadmium oxide (CdO, 99.999%), trioctylphosphine (TOP, 97%) and elemental  
43  
44 tellurium (Te, 99.99%) were purchased from Strem Chemicals. Copper (II) acetylacetonate  
45  
46 (Cu(C<sub>5</sub>H<sub>7</sub>O<sub>2</sub>)<sub>2</sub>, 99.99%), octylamine (99%), oleylamine (70%), oleic acid (90%), 1-octadecene  
47  
48 (90%), 1-octanethiol (C<sub>8</sub>SH, 98.5%), 1-dodecanethiol (C<sub>12</sub>SH, 98%), and 1-octadecanethiol  
49  
50 (C<sub>18</sub>SH, 98%), anhydrous ethanol and toluene were purchased from Sigma-Aldrich. All  
51  
52 chemicals were used without further purification.  
53  
54  
55  
56  
57  
58  
59  
60

1  
2  
3 **Synthesis of copper telluride nanodisks.** Copper telluride nanodisks were prepared by  
4 modification of a routine reported for the synthesis of spherical nanocrystals.<sup>24</sup> In detail, a  
5 trioctylphosphine-Te solution (TOPTe, typically 10w% Te in TOP, *i.e.* molar TOP/Te ratio of  
6 3:1) was prepared first, by dissolving Te powder in TOP at 250 °C under nitrogen for 3 hours,  
7 until the Te completely dissolved. The TOPTe solution was subsequently cooled to room  
8 temperature before use in the synthesis. In another flask, a mixture of 1.0 mmol of copper  
9 acetylacetonate (262 mg), 5 mL of C<sub>12</sub>SH, and 10 mL of oleic acid were heated to 100 °C and  
10 kept for 60 min under vacuum to prepare the copper precursor. Hereafter, the temperature was  
11 raised to 180 °C to form a clear solution. Once the temperature stabilized, 640 mg of the 10w%  
12 TOPTe solution was quickly injected. The reaction was kept at 180 °C for 2 min and then cooled  
13 to 80 °C. At this temperature, 1 mL of octylamine and 2 mL toluene were added to improve the  
14 colloidal stability of the nanodisks and further quench the reaction. Purification of the nanodisks  
15 was performed by adding an excess of ethanol to precipitate them, followed by centrifugation  
16 and resuspension in toluene. This process was repeated to ensure complete removal of excess  
17 ligands and unreacted precursors. To control the nanodisk diameter and thickness, we varied the  
18 reaction time and temperature, precursor concentrations, and the thiol ligand length.

19  
20  
21  
22  
23  
24  
25  
26  
27  
28  
29  
30  
31  
32  
33  
34  
35  
36  
37  
38  
39  
40  
41  
42 **Cation exchange reaction to CdTe quantum disks.** CdTe quantum disks were obtained by  
43 cation exchange reaction from copper telluride, according to previously reported approaches.<sup>27,28</sup>  
44 In order to perform the exchange, a Cd cation solution was prepared separately by dissolving 1  
45 mmol of CdO powder in a mixture of 4 mmol of oleic acid and 4 mL of octadecene at 240 °C,  
46 until we obtained a transparent solution. Hereafter, the solution was cooled to 180 °C, and the  
47 copper telluride nanodisks dispersed in TOP were swiftly injected into the cadmium oleate  
48 solution (Cd/Cu molar ratio of 100:1). TOP is an important chemical in cation exchange  
49  
50  
51  
52  
53  
54  
55  
56  
57  
58  
59  
60

1  
2  
3 reactions based on copper chalcogenides templates. As it is a soft base with a strong tendency to  
4 bind to copper ions, it can efficiently extract copper from the lattice.<sup>18</sup> The reaction proceeded  
5 for 5 minutes, during which we observed a change in color from the typical brown of copper  
6 telluride into dark red, indicating a successful exchange. After synthesis, the samples were  
7 purified by adding an excess of ethanol to precipitate the obtained CdTe quantum disks, and they  
8 were finally redispersed in toluene.  
9

10  
11  
12 **Structural characterization and elemental analysis.** X-ray diffraction patterns were collected  
13 with a Smartlab 9 kW Rigaku diffractometer equipped with a copper rotating anode. Samples  
14 were prepared by dropcasting of a nanocrystal suspension onto a Si(111) miscut substrate  
15 (7° toward the (110) plane). Bright-field transmission electron microscopy (BF-TEM) images  
16 and selected area electron diffraction (SAED) patterns were acquired using a 100kV JEOL JEM-  
17 1011 microscope. For the determination of the nanodisks diameter and thickness, typically 100-  
18 200 particles were measured. High-resolution TEM (HRTEM) images were obtained in a 200 kV  
19 ultra-high-resolution microscope (JEOL JEM-2200FS) equipped with a field emission gun, and a  
20 CEOS image aberration corrector. High angle annular dark field (HAADF) images, acquired in  
21 scanning TEM (STEM) mode, and energy dispersive X-ray spectroscopy (EDS) analyses were  
22 performed on the same instrument, with a Bruker Quantax 400 system with a 60 mm<sup>2</sup> XFlash  
23 5060 silicon drift detector. For HRTEM analyses, nanocrystal dispersions were drop-cast onto  
24 copper grids covered with an ultrathin amorphous carbon film suspended onto a lacey carbon  
25 net, while for EDS analysis they were deposited onto carbon-coated aluminum grids and the  
26 measurements were carried out using a holder with a beryllium cup. HAADF-STEM (annular  
27 aperture of 46 mrad, probe size 1 nm) was used because of the dominating incoherent nature of  
28 its signal, permitting to identify the shape of the nanocrystals by the inspection of their profiles  
29  
30  
31  
32  
33  
34  
35  
36  
37  
38  
39  
40  
41  
42  
43  
44  
45  
46  
47  
48  
49  
50  
51  
52  
53  
54  
55  
56  
57  
58  
59  
60

1  
2  
3 in the HAADF-STEM images. Simulations of the HAADF-STEM profiles were carried out  
4  
5 using the software STEM-CELL.<sup>29</sup>  
6  
7

8  
9 The X-ray photoelectron (XPS) characterization was performed on a Kratos Axis Ultra DLD  
10 spectrometer, using a monochromatic Al K $\alpha$  source (15kV, 20mA). Samples for XPS were  
11 prepared by drop casting 20  $\mu$ L of a solution containing the nanodisks on a highly oriented  
12 pyrolytic graphite (HOPG) substrate. High resolution narrow scans were performed at a constant  
13 pass energy of 10 eV and steps of 0.1 eV. The photoelectrons were detected at a take-off angle  $\Phi$   
14 = 0 $^\circ$  with respect to the surface normal. The pressure in the analysis chamber was maintained  
15 below  $7 \times 10^{-9}$  Torr for data acquisition. The binding energy (BE) scale was internally referenced  
16 to the C 1s peak (BE for C-C = 284.8 eV). Inductively coupled plasma optical emission  
17 spectroscopy (ICP-OES) was performed on a Thermo Scientific iCAP 6500 spectrometer.  
18 Samples for the ICP analysis were prepared by digestion of the dried nanodisks with aqua regia  
19 for 12 hours, followed by dilution with Milli-Q water.  
20  
21  
22  
23  
24  
25  
26  
27  
28  
29  
30  
31  
32  
33  
34  
35

36 **Optical spectroscopy.** Absorption spectra were recorded with a Varian Cary 5000 UV-vis-NIR  
37 absorption spectrophotometer. The emission was collected using an Edinburgh Instruments  
38 FLS920 spectrofluorometer. Samples were dried and dispersed in chloroform, with an optical  
39 density of about 0.1 cm $^{-1}$  at 500 nm. The PL quantum efficiency of the CdTe quantum disks was  
40 measured with an integrating sphere, exciting the samples at 500 nm. The lifetime was collected  
41 via time-correlated single-photon counting, exciting the sample at 400 nm with a 50 ps laser  
42 diode at a repetition rate of 1 MHz to ensure complete decay of the emission between the  
43 excitation pulses. The emission was measured at the peak position, with a typical emission band  
44 width of 4 nm. For the spectral dependence, a band width of 2 nm was used.  
45  
46  
47  
48  
49  
50  
51  
52  
53  
54  
55  
56  
57  
58  
59  
60



## Results and Discussion

Figure 1 shows typical TEM images of the copper telluride nanodisks. The average diameter and thickness are 10.1 nm and 2.3 nm, respectively, with a corresponding size dispersion (standard deviation) of 0.7 nm and 0.2 nm (histograms are shown in figure 1c and figure 1d). Due to the narrow size distributions, we can observe spontaneously assembled face-to-face disks standing on their edge on the TEM grid. By adding a non solvent (acetonitrile) to the solution as described in our previous paper on the assembly of branched NCs,<sup>30</sup> we could even induce large-area formation of face-to-face nanoribbons and superlattices thereof, which confirms the size homogeneity throughout the sample (see supporting information, figure S1).

The XPS characterization (figure 2a-c) yields a Cu/Te stoichiometry of 2.2:1. This ratio is confirmed by ICP-OES measurements which yield 2.1:1, and indicates the formation of quasi-stoichiometric  $\text{Cu}_2\text{Te}$ , with a slight Cu excess probably located at the nanodisk surface. Additionally, the Auger parameter for Cu, calculated as the sum of the binding energy of Cu  $2p_{3/2}$  peak (BE Cu  $2p_{3/2}$  =  $932.3 \pm 0.1$  eV, panel a) and of the kinetic energy of the Cu LMM Auger peak (KE Cu LMM = 917.6 eV, panel b), is equal to 1849.9 eV, in agreement with data already reported for Cu(I) chalcogenides,<sup>31</sup> and no satellites typical of Cu(II) species are observed (figure 2a). The positions of the Te  $3d_{5/2}$  and Te  $3d_{3/2}$  peaks, shown in panel b, are at 572.2 eV and 582.6 eV, respectively, in agreement with values reported for the (-2) oxidation state of Te.<sup>27</sup> Both results further support the formation of pure  $\text{Cu}_2\text{Te}$ , free from copper-deficient  $\text{Cu}_{(2-x)}\text{Te}$ ,  $0 < x \leq 1$ . Moreover, since no Te  $3d_{5/2}$  peaks are present around 576 - 577 eV, we can also exclude the presence of tellurium oxides (Te  $3d_{5/2}$  BE for  $\text{TeO}_2$ :  $575.9 \pm 0.2$  eV; Te

1  
2  
3 3d<sub>5/2</sub> BE for TeO<sub>3</sub>: 577 ± 0.3 eV.<sup>32</sup> In panel c, the XPS results collected on the Te 4s and S 2p  
4 peaks are reported. A quantitative analysis yields a S/Te ratio of 0.2:1, in line with the ratio  
5  
6 obtained from EDS (0.3:1 in the sample shown in figure 2d), and ICP-OES, where we found an  
7  
8 average S/Te ratio of 0.24:1 by evaluation of seven Cu<sub>2</sub>Te samples. Both results indicate the  
9  
10 presence of C<sub>12</sub>SH ligands bound to the surface of the nanodisks.  
11  
12  
13  
14  
15

16 XRD diffractograms recorded at room temperature on the Cu<sub>2</sub>Te nanodisks did not yield a  
17  
18 clear pattern (figure S2). Briefly annealing the sample at 100 °C in vacuum however  
19  
20 significantly improved the result, as the sharp reflections, probably arising from organic  
21  
22 impurities, were removed (figure 3a). The remaining pattern corresponded to a Cu<sub>2</sub>Te  
23  
24 nanocrystal possessing a hexagonal crystal symmetry (P6/mmm space group, ICSD structure no.  
25  
26 77055). Results were confirmed by measuring the SAED pattern of a collection of Cu<sub>2</sub>Te  
27  
28 nanodisks at room temperature. The integrated signal again shows a good match with the same  
29  
30 Cu<sub>2</sub>Te crystal structure (figure 3a). The SAED pattern is also in agreement with the (room-  
31  
32 temperature) HRTEM measurements, which exhibit single-crystal nanodisks of the same phase  
33  
34 (figure 3b-d). The data further revealed that the [001] direction is oriented perpendicular to the  
35  
36 plane of the Cu<sub>2</sub>Te nanodisks, similar to the case of Cu<sub>2</sub>S nanodisks reported by Sigman *et al.*<sup>10</sup>  
37  
38  
39  
40  
41  
42

43 The average thickness and diameter of as-synthesized Cu<sub>2</sub>Te nanodisks can be tuned by  
44  
45 changing the growth time and temperature, and the concentration of the TOPTe solution. In  
46  
47 general, higher temperatures resulted in thicker nanodisks, yet with a smaller diameter. For  
48  
49 instance, Cu<sub>2</sub>Te nanodisks with a thickness of 2.2 nm and a diameter of 12 nm were prepared at a  
50  
51 temperature of 175 °C. By increasing it a mere 10 °C, the diameter was reduced to 8 nm and the  
52  
53 thickness increased to 3.2 nm. Interestingly, a lower and higher limit for the temperature was  
54  
55 observed at 160 °C and 200 °C, respectively, where in both cases spherical nanocrystals were  
56  
57  
58  
59  
60

1  
2  
3 obtained, with diameters of 4.6 nm (supporting information, figure S3a) and 7.4 nm (supporting  
4 information, figure S3b), respectively. Elemental analysis via ICP-OES yielded an elevated  
5 concentration of sulfur in the latter case (atomic ratio of S/Te equal to 1.2:1), due to the  
6 decomposition of C<sub>12</sub>SH at 200 °C. This is consistent with reported results that C<sub>12</sub>SH can be  
7 used as sulfur source to prepare monodisperse copper sulfide nanocrystals at a temperature of  
8 230 °C.<sup>33</sup>  
9  
10  
11  
12  
13  
14  
15  
16  
17

18 Reducing the Te concentration to 5w% (thus injecting a larger amount of TOPTe to maintain a  
19 constant Cu/Te ratio) also suppressed the formation of nanodisks at 180 °C (supporting  
20 information, figure S4). Higher concentrations of Te (*i.e.* 15w% TOPTe) on the other hand  
21 facilitated the formation of nanodisks with larger lateral dimensions (12 nm diameter *vs.* 8 nm as  
22 described above). It is clear that the experimental conditions (temperature, ligand length,  
23 precursor concentrations) to obtain Cu<sub>2</sub>Te nanodisks of uniform size and shape lie in a narrow  
24 range. Even when varying the thiol chain length using C<sub>8</sub>SH, C<sub>12</sub>SH, or C<sub>18</sub>SH, we only  
25 observed the formation of nanodisks for C<sub>12</sub>SH (supporting information, figure S5).  
26 Nevertheless, under the appropriate conditions, high quality Cu<sub>2</sub>Te can be readily synthesized,  
27 with a typical diameter varying between 8 and 12 nm, and a thickness between *ca.* 2 and 3.5 nm  
28 (see table S1 for a summary of synthesis conditions).  
29  
30  
31  
32  
33  
34  
35  
36  
37  
38  
39  
40  
41  
42  
43  
44

45 In agreement with earlier literature results on spherical and rod-like nanocrystals,<sup>27,28,34</sup> the Cu<sup>+</sup>  
46 cations could be exchanged to Cd<sup>2+</sup> while maintaining the shape of the nanocrystals. Figures 4a-  
47 b show HAADF-STEM images, including a side view of some CdTe nanodisks adhered to the  
48 walls of the lacey grid. The intensity profiles determined from the HAADF-STEM images  
49 (figure 4c) also matched well with a simulated profile from an ideal nanodisk with flat surfaces.  
50  
51  
52  
53  
54  
55  
56  
57  
58  
59  
60

1  
2  
3 Interestingly, in contrast with the typical Cd- to Cu- exchange reaction proceeding swiftly  
4 under ambient room temperature conditions,<sup>35</sup> here we needed to raise the temperature before a  
5 cation exchange was observed. Indeed, when adding a 30-fold excess of Cd-oleate to a solution  
6 of Cu<sub>2</sub>Te nanodisks and keeping it for 24 hours at 50 °C, the chemical composition (obtained via  
7 ICP-OES) did not show any substantial incorporation of Cd into the lattice (table 1). At a  
8 temperature of 100 °C, a partial exchange was obtained after 60 minutes. A further increase of  
9 the temperature to 150 °C resulted in a nearly-complete exchange in 5 minutes, with finally less  
10 than 1% of Cu typically remaining at 200 °C. Above this temperature, full exchange occurred,  
11 yet at the expense of a reshaping of the particles into spherical CdTe nanocrystals (supporting  
12 information, figure S6).  
13  
14  
15  
16  
17  
18  
19  
20  
21  
22  
23  
24  
25  
26  
27

Temperature	Reaction time	Final Cd/Cu Ratio
50 °C	24 hours	4 %
100 °C	1 hour	52 %
150 °C	5 mins	97 %
200 °C	5 mins	99.3%

28  
29 Table 1: The exchange efficiency was evaluated by performing the cation exchange reactions  
30 at different temperatures, followed by ICP-OES analysis of the chemical composition of the  
31 obtained nanocrystals. For these reactions, we added a 30-fold excess of Cd-precursors,  
32 compared to the total amount of Cu atoms present. The reactions above 100 °C were stopped  
33 after 5 min.  
34  
35  
36  
37  
38  
39  
40  
41  
42  
43  
44  
45  
46  
47  
48  
49

50  
51 Cation exchange reactions occurring at elevated temperatures have been observed in other  
52 systems. For instance, previously we performed cation exchange reactions at 250 °C to  
53 completely remove residual copper ions from ZnSe/ZnS quantum rods, in order to obtain  
54  
55  
56  
57  
58  
59  
60

1  
2  
3 efficient band edge luminescence.<sup>28,34</sup> Beberwyck *et al.* reported the preparation of III-V InP and  
4 InAs nanocrystals via an ion exchange reaction from Cd<sub>3</sub>P<sub>2</sub> or Cd<sub>3</sub>As<sub>2</sub>, respectively, wherein a  
5 temperature of 300 °C was necessary to induce the exchange in the strongly bound covalent  
6 lattice.<sup>19</sup> IV-VI PbX (X=S, Se, Te) nanocrystals can be passivated with an outer shell of CdX via  
7 cation exchange, yet also here the temperature needs to be raised over 100 °C before a reaction  
8 occurs, above which the shell thickness is mainly determined by the growth temperature.<sup>36,37</sup>  
9  
10  
11  
12  
13  
14  
15  
16  
17  
18

19 After the cation exchange reaction, we obtained crystalline CdTe nanodisks with a Cd/Te  
20 atomic ratio of 1.3:1 (measured with EDS, figure 4d) and a wurtzite crystal structure (space  
21 group P6<sub>3</sub>mc, JCPDS Card no. 01-0732871, figure 4e). However, the XRD pattern showed an  
22 especially narrow peak for the (002) reflection, suggesting that the *c*-axis now lies in the  
23 nanodisk plane. Note that a second narrow peak for the (004) reflection should be observed,  
24 however, the intensity of the (004) reflection in bulk wurtzite CdTe is only 0.1% compared to the  
25 highest intensity (JCPDS Card no. 01-0732871), hence this peak is not discernible in our XRD  
26 pattern. From the line width of the (002) reflection, the Scherrer equation  $D = K\lambda/(\beta\cos\theta)$ , with  
27 *D* the crystallite size,  $\lambda$  the X-ray wavelength,  $\beta$  the full width at half maximum of the diffraction  
28 peak,  $\theta$  the Bragg angle and  $K = 0.9$ , yields a crystallite coherence length of 8.1 nm along the  
29 [001] direction (see supporting information, figure S10). Applying the Scherrer equation to the  
30 width of the (110) peak results in a 2.8 nm size along the [110] direction. The other XRD  
31 reflections yield sizes ranging from 2.8 to 3.3 nm, with slight variation due to the different  
32 directions probed. Data are in agreement with the TEM images, where we obtained an average  
33 diameter of 10 nm and a thickness of 2.9 nm. The peculiar orientation of the CdTe quantum  
34 disks was further confirmed by the measurement of the crystal structure on single disks using  
35  
36  
37  
38  
39  
40  
41  
42  
43  
44  
45  
46  
47  
48  
49  
50  
51  
52  
53  
54  
55  
56  
57  
58  
59  
60

1  
2  
3 HRTEM (figures 4f-g). The images give direct evidence that the [001] direction lies in the plane  
4  
5 of the nanodisks.  
6  
7

8  
9 In the present study, as the cation exchange is conducted on anisotropic nanocrystals, we are  
10 given a unique insight into the exchange mechanism. Knowing that the exchange occurs between  
11 hexagonal crystals with highly similar lattice constants ( $a_1=4.23\text{\AA}$  and  $c_1=7.27\text{\AA}$  for  $\text{Cu}_2\text{Te}$ ,  
12 ICSD structure # 77055, and  $a_2=4.57\text{\AA}$  and  $c_2=7.47\text{\AA}$  for CdTe, JCPDS Card no. 01-0732871)  
13 yet with different orientation of the  $c$ -axis (figure 5a), we compared the underlying Te sublattice  
14 before and after exchange. Figures 5b-c clearly show that the exchange can only occur when it is  
15 accompanied by slight displacements of the Te anions, to accomplish the evolution from  $\text{Cu}_2\text{Te}$   
16 disks terminated by (001) basal planes to CdTe disks terminated by (110) basal planes. First we  
17 note that in both structures the Te atoms form separate columns when viewed from the (flat) top,  
18 *i.e.* there is no mixing with cations in the columns. Let us consider then the four Te atoms in the  
19 (001) plane in  $\text{Cu}_2\text{Te}$  (magenta atoms in figure 5b-c). These Te anions shift position in CdTe,  
20 with two atoms staying on the new (110) plane, and two atoms moving down (or equivalently  
21 up) to form the second (110) plane in CdTe. The in-plane displacements are quite small (about  
22 0.3 Å) resulting in a slight distortion of the projected hexagonal Te lattice (giving an in-plane  
23 projected area compressed by about 5%). The main displacements are along the  $z$  direction,  
24 resulting in a splitting of a pristine (001) Te-plane of  $\text{Cu}_2\text{Te}$  into the (110) Te ‘bilayer’ of CdTe.  
25 Considering also the Te atoms from the layers underneath, the average displacement per Te atom  
26 along  $z$  is about 1.9 Å (given by the difference  $2a_2 - c_1$ ).  
27  
28  
29  
30  
31  
32  
33  
34  
35  
36  
37  
38  
39  
40  
41  
42  
43  
44  
45  
46  
47  
48  
49  
50

51  
52 This reconstruction effectively tilts the  $c$ -axis into the plane of the nanodisks, and additionally  
53 leads to an overall increase in thickness of about 25% after cation exchange. To verify this, we  
54 measured the thickness in a sample of  $\text{Cu}_2\text{Te}$  nanodisks, and the corresponding CdTe disks. We  
55  
56  
57  
58  
59  
60

1  
2  
3 obtained (1.85±0.09) nm and (2.26±0.10) nm for the average thickness of Cu<sub>2</sub>Te and CdTe,  
4  
5 respectively, suggesting an increase in thickness of 22% (errors represent 95% confidence  
6  
7 intervals). Two other samples yielded (2.30±0.14) nm vs. (2.11±0.13) nm (8% decrease), and  
8  
9 (2.38±0.11) nm vs. (2.92±0.17) nm (23% increase), respectively. Hence, in agreement with the  
10  
11 calculations, the TEM measurements suggest an increase in thickness of about 12%. The  
12  
13 experimental observations and corresponding modeling show that changes are small enough to  
14  
15 maintain the overall shape of the nanocrystal, yet they are likely sufficient to lead to the  
16  
17 temperature-activation of the exchange reaction, as it implies that the exchange requires  
18  
19 sufficient thermal energy for the atoms to hop to the new lattice sites. While a complete  
20  
21 clarification of the driving force behind the reconstruction requires further total energy  
22  
23 calculations, computational studies on bulk facets of wurtzite CdSe have already shown that  
24  
25 most ligands have higher binding affinities for the non-polar (100) and (110) facets in this  
26  
27 material than for the (001) and (00-1) facets,<sup>38,39</sup> so that in general the non-polar facets in  
28  
29 surfactant-passivated NCs tend to have a lower surface energy and consequently a larger surface  
30  
31 area than the polar ones. A similar situation should apply here, aided by the possibility for the  
32  
33 lattice to reorganize during cation exchange, under the constraint of overall preservation of the  
34  
35 crystal shape. Such reorganization, favored by the high temperature at which the exchange is  
36  
37 performed, appears to drive the system to a low-energy configuration characterized by CdTe  
38  
39 nanodisks that are terminated by large (110) and (-110) top and bottom facets. Considering that  
40  
41 cation exchange reactions often occur between different crystal structures (*e.g.* monoclinic Cu<sub>2</sub>S  
42  
43 to cubic PbS),<sup>40</sup> or that even structures sharing the same anion sublattice (*e.g.* PbX to CdX)<sup>37,41</sup>  
44  
45 have shown distortions, our results on shape-controlled nanocrystals may therefore aid in a better  
46  
47 understanding of cation exchange mechanism in other materials systems.  
48  
49  
50  
51  
52  
53  
54  
55  
56  
57  
58  
59  
60

1  
2  
3 To ensure maximal removal of the Cu atoms while maintaining the nanodisk shape, we  
4 determined the optimal temperature for the cation exchange reaction to be around 180 °C. Under  
5 this condition, we synthesized a series of CdTe disks with a red emission that could be tuned  
6 continuously from 600 nm to 640 nm. Figure 6a shows a typical absorption and emission  
7 spectrum, for 10 nm by 2.9 nm CdTe quantum disks, with a series of PL spectra displayed in  
8 figure 6(b). PL spectra are typically slightly broader (*e.g.* 35 nm full width at half maximum,  
9 FWHM, in figure 6a) than those obtained for spherical CdTe quantum dots (supporting  
10 information, figure S8), with a small tail toward red wavelengths. This is most likely due to the  
11 small thickness and the concurring enhanced sensitivity to size dispersion originating from the  
12 strong quantum confinement in this direction. Indeed, a PL excitation spectrum confirms that the  
13 typical homogeneous line width at room temperature equals 22 nm (FWHM, for a sample  
14 emitting at 637 nm), leading to a substantially narrower peak than the 32 nm ensemble-  
15 broadened band-edge absorption (supporting information figure S9).  
16  
17  
18  
19  
20  
21  
22  
23  
24  
25  
26  
27  
28  
29  
30  
31  
32  
33  
34

35 Figure 6c shows that the PL peak position is correlated with the quantum disk thickness (see  
36 also supporting information table S2). Note that we used the thickness of the corresponding  
37 Cu<sub>2</sub>Te nanodisks to plot the data, as the CdTe typically lie flat on the TEM grid, while the Cu<sub>2</sub>Te  
38 disks easily form aligned stacks allowing an accurate thickness determination (see figure 1 and  
39 figure S1). Furthermore, the average, size-independent increase of about 12% (*cf.* above) is not  
40 expected to affect the overall trend observed in figure 6c. In contrast, no correlation is observed  
41 with the disk diameter (supporting information figure S10). This does not come unexpected: as  
42 the typical diameters are only slightly smaller than the 13.4 nm exciton Bohr diameter in CdTe,  
43 confinement effects arising from the small thickness should form the dominant contribution to  
44 the PL blue shift.  
45  
46  
47  
48  
49  
50  
51  
52  
53  
54  
55  
56  
57  
58  
59  
60



1  
2  
3 We measured the PL quantum efficiency (QE) for 8 samples, and found an average value of  
4 18.1%, and a peak value of 36% (table 2). The table also shows that Cu/Cd atomic ratios fell  
5 well below 1% for all but two samples, supporting the assignment of the PL to band-edge  
6 exciton recombination. Comparing the different QE values, no quenching of the band-edge PL  
7 with increasing Cu concentration is observed over the different samples, however, it is known  
8 that in Cu-doped Zn and Cd chalcogenides, the quenching is weakest in CdTe, possibly due to  
9 the energetic position of the Cu-level, only 0.15 eV above the valence band of CdTe (whereas in  
10 other materials Cu yields deep trap state).<sup>42</sup> The quenching might even be further suppressed by a  
11 permanent hole present in the Cu-dopant, preventing nonradiative hole relaxation,<sup>43</sup> although this  
12 remains to be investigated.  
13  
14  
15  
16  
17  
18  
19  
20  
21  
22  
23  
24  
25  
26  
27

28 We are not yet at the level of recent results obtained on CdSe core/graded shell quantum dots  
29 with efficiencies exceeding 80% in solid state conditions,<sup>44</sup> however, the QE values can still be  
30 considered an excellent starting point for further spectroscopic investigations. Moreover, the  
31 CdTe quantum disks show an enhanced stability of the PL when stored under ambient conditions  
32 compared with their spherical counterparts synthesized by a conventional approach.<sup>45</sup> While the  
33 latter quantum dots already loose more than 90% of their initial PL after 60 hours, the CdTe  
34 quantum disks reported here, despite their larger surface-to-volume ratio, retain 60% of their  
35 luminescence even after 10 days (figure 6d). The reason is the efficient passivation of the  
36 surface. XPS results collected on the CdTe quantum disks show an S/Te ratio of 0.25/1, in  
37 agreement with the parent Cu<sub>2</sub>Te nanodisks. However, detailed investigation shows that these S  
38 atoms behave differently for Cu<sub>2</sub>Te and CdTe when exposed to prolonged X-ray irradiation  
39 (figure S11). In the case of Cu<sub>2</sub>Te, the S 2p peak intensity and hence the sulfur concentration  
40 decreased with time due to X-ray-induced damage and removal of the thiol capping layer.<sup>46</sup> On  
41  
42  
43  
44  
45  
46  
47  
48  
49  
50  
51  
52  
53  
54  
55  
56  
57  
58  
59  
60

the other hand, for CdTe nanodisks the intensity of the S 2p peak remained constant. A deconvolution of the S 2p peak gives more insight into nature of the chemical bonds (figure S11c). In the case of the Cu<sub>2</sub>Te nanodisks, a good fit was obtained with one doublet, fixing the position of the S 2p<sub>3/2</sub> peak at  $162 \pm 0.2$  eV typical for thiols adsorbed on Cu.<sup>47</sup> On the other hand, in the case of CdTe quantum disks two doublets were needed. In particular, the doublet with higher intensity corresponds to about 89% of the total S content (green curves in panel c), and it is centered at  $161.2 \pm 0.2$  eV, a value typical for CdS.<sup>48</sup> The XPS analysis therefore suggests that, during the cation exchange reaction, the majority of the S atoms in the thiol capping layer bind tightly to the excess Cd on the quantum disk surface, forming an effective monolayer of CdS. This protects the CdTe core from oxidation, leading to the enhanced PL stability.

sample	Cu/Cd ratio (%)	PL (nm)	QE (%)
CdTe_1	0.3	616.4	8.00
CdTe_2	0.09	621.7	14.7
CdTe_3	3	630.0	20.3
CdTe_4	0.03	621.8	31.3
CdTe_5	0.06	636.6	6.00
CdTe_6	2	637.3	36.1
CdTe_7	<sup>(1)</sup>	603.0	17.2
CdTe_8	<sup>(1)</sup>	637.7	11.5

Table 2. Cu/Cd atomic ratio (determined by ICP-OES), PL peak position and quantum efficiency of the eight samples investigated. <sup>(1)</sup>For 2 additional samples, the PL QE was measured without determination of the Cu/Cd ratio.

1  
2  
3 Finally, the band-edge PL lifetime was measured using time-resolved fluorescence  
4 spectroscopy. A typical trace is shown in figure 7a, for CdTe disks with a 616 nm peak emission.  
5  
6 The dominant component of the decay has a lifetime of 9 ns (lifetime-weighted relative  
7 amplitude of 65%), yet we used a tri-exponential decay function in order to adequately fit  
8 smaller-weight components with a shorter (1.5 ns, 2%) and longer (23 ns, 33%) lifetime,  
9 respectively. Figure 7b shows the spectral dependence of the decay. Averaged over all traces,  
10 typical decay times (figure 7c) and weights corresponded to  $3 \pm 1.5$  ns (5%),  $12 \pm 2$  ns (62%)  
11 and  $31 \pm 7$  ns (33%), similar to the decay times at the peak position (figure 7a). Values increased  
12 to  $8 \pm 2$  ns (13%),  $20 \pm 3$  ns (62%) and  $59 \pm 7$  ns (25%), respectively, for CdTe disks with a 637  
13 nm peak emission. Most importantly, in both cases we did not observe the typical long lifetime  
14 of several 100 ns associated with Cu-related emission in metal chalcogenide nanocrystals,<sup>49-52</sup> in  
15 agreement with the limited Cu-concentration measured via elemental analysis.  
16  
17  
18  
19  
20  
21  
22  
23  
24  
25  
26  
27  
28  
29  
30  
31

32  
33 Figure 7d displays the weighted average decay time for eight CdTe quantum disk samples.  
34 Data are consistently smaller than those obtained on spherical quantum dots. The latter fall in the  
35 range of 17 ns to 25 ns and agree well with literature values,<sup>53</sup> where also a band-gap dependence  
36 is reported by following equation:  $\tau = (-0.0903 + 0.066 \cdot 1239.85/\lambda_0)^{-1}$ ,<sup>54</sup> with  $\tau$  the exciton lifetime  
37 and  $\lambda_0$  the spectral position of the PL peak (figure 7d, dashed line). The PL lifetime of the disks  
38 is more scattered, yielding a band that is approximately 25-45% faster than the spherical Qdots.  
39  
40  
41  
42  
43  
44  
45  
46  
47

48 The emission rate  $\tau^{-1}$  at a given frequency  $\omega$  is directly proportional to the local field factor  
49  $|f_{LF}|^2$  expressing the dielectric screening of the incident and emitted light, and the effective band-  
50 edge oscillator  $f_{if}$  strength, taking the exciton distribution over different dark and bright states  
51 into account.<sup>55-57</sup>  
52  
53  
54  
55  
56  
57  
58  
59  
60

$$\tau^{-1} = \frac{e^2}{2\pi\epsilon_0 c^3 m_e} n_s |f_{LF}|^2 \omega^2 f_{if},$$

$$f_{if} = \frac{\sum_k f_k \cdot \exp(-\frac{\Delta E_k}{kT})}{\sum_k g_k / g \cdot \exp(-\frac{\Delta E_k}{kT})} \quad (1)$$

$\epsilon_0$  equals the dielectric constant, and for each state  $k$ ,  $f_k$ ,  $g_k$ , and  $\Delta E_k$  are the oscillator strength, degeneracy and energetic splitting from the lowest excited state, respectively ( $g$ : total band gap degeneracy). A full quantification of the emission rate is beyond the scope of the present manuscript; however, eq. (1) already gives important indications for the faster  $\tau^{-1}$  in Qdisks. Firstly, the strong confinement of the disks in the lateral dimension allows for a larger nanocrystal volume at a given emission wavelength (see supporting information, figure S10). In line with the increase of the oscillator strength with volume observed for spherical Qdots,<sup>57,58</sup> at a given emission wavelength we expect  $f_{if}$  to be larger in the disks leading to a faster  $\tau^{-1}$ . The peculiar shape will also affect the dielectric screening<sup>55</sup> (see supporting information). We calculated a band-edge  $|f_{LF}|^2 = 0.216$  and  $|f_{LF}|^2 = 0.308$  for Qdots and Qdisks, respectively, again favoring a faster emission rate in the Qdisks.

To a certain extent, both may be compensated by the different band-edge states populated at room temperature, as it is known that the shape can also substantially modify the splitting between them.<sup>59,60</sup> Nevertheless, the results point toward a convenient control of the emission lifetime via the shape of the nanocrystals, in this case inducing a faster recombination rate. This is for instance beneficial for the design of efficient single (quantum) emitters,<sup>61</sup> as it enhances the single dot brightness.

## Conclusions

We have synthesized novel disk-shaped  $\text{Cu}_2\text{Te}$  nanocrystals with a tunable diameter and thickness and a hexagonal crystal structure. Subsequent cation exchange from Cu to Cd at high temperature (180 °C) enabled us to obtain highly fluorescent CdTe nanocrystals, with typically less than 1% of Cu (compared to Cd) remaining in the lattice. While cation exchange reactions maintain the overall shape of the nanocrystal as is also the case here, our data showed that they can still imply a substantial restructuring of the anion sublattice. Detailed analysis of the PL lifetime in the resulting CdTe quantum disks allowed us to conclude that it arises from band-edge exciton recombination, and the emission related to Cu-impurity levels was not observed. The PL lifetime was *ca.* 25-45% faster than those of spherical quantum dots at the same emission wavelength. Absolute values of the fluorescence quantum efficiency reached up to 36%, with an average of 18% over eight different samples prepared in similar way. Given their peculiar shape as well as the in-plane orientation of the *c*-axis, and taking into account that present quantum efficiencies could still be further enhanced by a development of core/shell nanocrystals, these novel nanostructures may spark a further investigation into the shape- and crystal structure dependent opto-electronic band structure of colloidal quantum dots, and find application in future photonic devices such as lasers,<sup>44</sup> LEDs<sup>62</sup> or quantum emitters.<sup>61</sup>

## ASSOCIATED CONTENT

**Supporting Information.** Synthesis protocols to obtain differently sized quantum disks, large-scale TEM image of self-assembled  $\text{Cu}_2\text{Te}$  nanodisks, and additional optical, electron

1  
2  
3 microscopy, X-ray diffraction and XPS data. This material is available free of charge via the  
4  
5 Internet at <http://pubs.acs.org>.  
6  
7  
8  
9

## 10 11 12 AUTHOR INFORMATION

### 13 14 15 **Corresponding Author**

16  
17 \* [iwan.moreels@iit.it](mailto:iwan.moreels@iit.it)  
18  
19

### 20 21 22 **Author Contributions**

23 The manuscript was written through contributions of all authors. All authors have given approval  
24  
25 to the final version of the manuscript. #These authors contributed equally to the manuscript.  
26  
27

### 28 29 30 **Funding Sources**

31 The European Union's 7th Framework Program, under REA grant agreement PIEF-GA-2011-  
32  
33 298022 and grant agreement 240111.  
34  
35  
36  
37

## 38 39 40 ACKNOWLEDGMENTS

41 F. De Donato, G. Pugliese and S. Nitti are acknowledged for collecting the ICP-OES data. The  
42  
43 research leading to these results has received funding from the European Union's Seventh  
44  
45 Framework Program (FP7/2007-2013) under REA grant agreement no. PIEF-GA-2011-298022  
46  
47 (NIRPLANA) and 240111 (ERC starting grant NANO-ARCH).  
48  
49  
50  
51  
52  
53  
54  
55  
56  
57  
58  
59  
60

## REFERENCES

- (1) Alivisatos, A. P. *Science* **1996**, *271*, 933-937.
- (2) Peng, X.; Schlamp, M. C.; Kadavanich, A. V.; Alivisatos, A. P. *Journal of the American Chemical Society* **1997**, *119*, 7019-7029.
- (3) Peng, X. G.; Manna, L.; Yang, W. D.; Wickham, J.; Scher, E.; Kadavanich, A.; Alivisatos, A. P. *Nature* **2000**, *404*, 59-61.
- (4) Dong, A.; Tang, R.; Buhro, W. E. *Journal of the American Chemical Society* **2007**, *129*, 12254-12262.
- (5) Carbone, L.; Nobile, C.; De Giorgi, M.; Sala, F. D.; Morello, G.; Pompa, P.; Hytch, M.; Snoeck, E.; Fiore, A.; Franchini, I. R.; Nadasan, M.; Silvestre, A. F.; Chiodo, L.; Kudera, S.; Cingolani, R.; Krahne, R.; Manna, L. *Nano Letters* **2007**, *7*, 2942-2950.
- (6) Ithurria, S.; Tessier, M. D.; Mahler, B.; Lobo, R. P. S. M.; Dubertret, B.; Efros, A. L. *Nature Materials* **2011**, *10*, 936-941.
- (7) Bouet, C.; Tessier, M. D.; Ithurria, S.; Mahler, B.; Nadal, B.; Dubertret, B. *Chemistry of Materials* **2013**, 1262-1271.
- (8) Cassette, E.; Mahler, B.; Guigner, J. M.; Patriarche, G.; Dubertret, B.; Pons, T. *ACS Nano* **2012**, *6*, 6741-6750.
- (9) Ithurria, S.; Talapin, D. V. *Journal of the American Chemical Society* **2012**, *134*, 18585-18590.
- (10) Sigman, M. B.; Ghezelbash, A.; Hanrath, T.; Saunders, A. E.; Lee, F.; Korgel, B. A. *Journal of the American Chemical Society* **2003**, *125*, 16050-16057.
- (11) Choi, J.; Kang, N.; Yang, H. Y.; Kim, H. J.; Son, S. U. *Chemistry of Materials* **2010**, *22*, 3586-3588.
- (12) Du, Y.; Yin, Z.; Zhu, J.; Huang, X.; Wu, X.-J.; Zeng, Z.; Yan, Q.; Zhang, H. *Nat. Commun.* **2012**, *3*, 1177.
- (13) Li, Z.; Peng, X. *Journal of the American Chemical Society* **2011**, *133*, 6578-6586.
- (14) Hu, S.; Wang, X. *Chem. Soc. Rev.* **2013**, *42*, 5577-5594.
- (15) Schliehe, C.; Juarez, B. H.; Pelletier, M.; Jander, S.; Greshnykh, D.; Nagel, M.; Meyer, A.; Foerster, S.; Kornowski, A.; Klinke, C.; Weller, H. *Science* **2010**, *329*, 550-553.
- (16) Saunders, A. E.; Ghezelbash, A.; Smilgies, D.-M.; Sigman, M. B.; Korgel, B. A. *Nano Letters* **2007**, *7*, 541-541.
- (17) Ithurria, S.; Dubertret, B. *Journal of the American Chemical Society* **2008**, *130*, 16504-16505.
- (18) Son, D. H.; Hughes, S. M.; Yin, Y. D.; Alivisatos, A. P. *Science* **2004**, *306*, 1009-1012.
- (19) Beberwyck, B. J.; Alivisatos, A. P. *Journal of the American Chemical Society* **2012**, *134*, 19977-19980.
- (20) Deka, S.; Miszta, K.; Dorfs, D.; Genovese, A.; Bertoni, G.; Manna, L. *Nano Letters* **2010**, *10*, 3770-3776.
- (21) Jain, P. K.; Amirav, L.; Aloni, S.; Alivisatos, A. P. *Journal of the American Chemical Society* **2010**, *132*, 9997-9999.
- (22) Sadtler, B.; Demchenko, D. O.; Zheng, H.; Hughes, S. M.; Merkle, M. G.; Dahmen, U.; Wang, L.-W.; Alivisatos, A. P. *Journal of the American Chemical Society* **2009**, *131*, 5285-5293.
- (23) Hsu, S.-W.; Bryks, W.; Tao, A. R. *Chemistry of Materials* **2012**, *24*, 3765-3771.

- 1  
2  
3 (24) Kriegel, I.; Jiang, C.; Rodríguez-Fernández, J.; Schaller, R. D.; Talapin, D. V.; da  
4 Como, E.; Feldmann, J. *Journal of the American Chemical Society* **2011**, *134*, 1583-1590.
- 5 (25) Kriegel, I.; Rodríguez-Fernández, J.; Wisnet, A.; Zhang, H.; Waurisch, C.;  
6 Eychmuller, A.; Dubavik, A.; Govorov, A. O.; Feldmann, J. *ACS Nano* **2013**, *7*, 4367-4377.
- 7 (26) Li, W.; Zamani, R.; Rivera\_Gil, P.; Pelaz, B.; Ibáñez, M.; Cadavid, D.; Shavel,  
8 A.; Alvarez-Puebla, R. A.; Parak, W. J.; Arbiol, J.; Cabot, A. *Journal of the American Chemical*  
9 *Society* **2013**, *135*, 7098-7101.
- 10 (27) Dilena, E.; Dorfs, D.; George, C.; Miszta, K.; Povia, M.; Genovese, A.; Casu, A.;  
11 Prato, M.; Manna, L. *Journal of Materials Chemistry* **2012**, *22*, 13023-13031.
- 12 (28) Li, H.; Brescia, R.; Krahne, R.; Bertoni, G.; Alcocer, M. J. P.; D'Andrea, C.;  
13 Scotognella, F.; Tassone, F.; Zanella, M.; De Giorgi, M.; Manna, L. *ACS Nano* **2012**, *6*, 1637-  
14 1647.
- 15 (29) Bertoni, G.; Grillo, V.; Brescia, R.; Ke, X.; Bals, S.; Catellani, A.; Li, H.; Manna,  
16 L. *ACS Nano* **2012**, *6*, 6453-6461.
- 17 (30) Miszta, K.; de Graaf, J.; Bertoni, G.; Dorfs, D.; Brescia, R.; Marras, S.;  
18 Ceseracciu, L.; Cingolani, R.; van Roij, R.; Dijkstra, M.; Manna, L. *Nature Materials* **2011**, *10*,  
19 872-876.
- 20 (31) Moulder, J. F.; Stickle, W. F.; Sobol, P. E.; Bomben, K. D. *Handbook of X-ray*  
21 *Photoelectron Spectroscopy, Perkin-Elmer Corp., Eden Prairie, MN, USA* **1992**.
- 22 (32) Carmona-Rodriguez, J.; Lozada-Morales, R.; del Angel-Vicente, P.; Jimenez-  
23 Sandoval, O.; Lopez-Calzada, G.; Dahlberg, D.; Jimenez-Sandoval, S. *Journal of Materials*  
24 *Chemistry* **2011**, *21*, 13001-13008.
- 25 (33) Choi, S. H.; An, K.; Kim, E. G.; Yu, J. H.; Kim, J. H.; Hyeon, T. *Adv. Funct.*  
26 *Mater.* **2009**, *19*, 1645-1649.
- 27 (34) Li, H.; Zanella, M.; Genovese, A.; Povia, M.; Falqui, A.; Giannini, C.; Manna, L.  
28 *Nano Letters* **2011**, *11*, 4964-4970.
- 29 (35) Rivest, J. B.; Jain, P. K. *Chemical Society Reviews* **2013**, *42*, 89-96.
- 30 (36) Justo, Y. *PhD Thesis Ghent University* **2012**, 9789461970893.
- 31 (37) Lambert, K.; Geyter, B. D.; Moreels, I.; Hens, Z. *Chemistry of Materials* **2009**,  
32 *21*, 778-780.
- 33 (38) Manna, L.; Wang; Cingolani, R.; Alivisatos, A. P. *The Journal of Physical*  
34 *Chemistry B* **2005**, *109*, 6183-6192.
- 35 (39) Rempel, J. Y.; Trout, B. L.; Bawendi, M. G.; Jensen, K. F. *The Journal of*  
36 *Physical Chemistry B* **2006**, *110*, 18007-18016.
- 37 (40) Luther, J. M.; Zheng, H.; Sadtler, B.; Alivisatos, A. P. *Journal of the American*  
38 *Chemical Society* **2009**, *131*, 16851-16857.
- 39 (41) Casavola, M.; van Huis, M. A.; Bals, S.; Lambert, K.; Hens, Z.; Vanmaekelbergh,  
40 D. *Chemistry of Materials* **2011**, *24*, 294-302.
- 41 (42) Grandhi, G. K.; Tomar, R.; Viswanatha, R. *Acs Nano* **2012**, *6*, 9751-9763.
- 42 (43) Viswanatha, R.; Brovelli, S.; Pandey, A.; Crooker, S. A.; Klimov, V. I. *Nano*  
43 *Letters* **2011**, *11*, 4753-4758.
- 44 (44) Dang, C.; Lee, J.; Breen, C.; Steckel, J. S.; Coe-Sullivan, S.; Nurmikko, A. *Nature*  
45 *Nanotechnology* **2012**, *7*, 335-339.
- 46 (45) Fiore, A.; Mastroia, R.; Lupo, M. G.; Lanzani, G.; Giannini, C.; Carlino, E.;  
47 Morello, G.; De Giorgi, M.; Li, Y.; Cingolani, R.; Manna, L. *Journal of the American Chemical*  
48 *Society* **2009**, *131*, 2274-2282.
- 49  
50  
51  
52  
53  
54  
55  
56  
57  
58  
59  
60



- 1  
2  
3  
4  
5  
6  
7  
8  
9  
10  
11  
12  
13  
14  
15  
16  
17  
18  
19  
20  
21  
22  
23  
24  
25  
26  
27  
28  
29  
30  
31  
32  
33  
34  
35  
36  
37  
38  
39  
40  
41  
42  
43  
44  
45  
46  
47  
48  
49  
50  
51  
52  
53  
54  
55  
56  
57  
58  
59  
60
- (46) Gonella, G.; Terreni, S.; Cvetko, D.; Cossaro, A.; Mattera, L.; Cavalleri, O.; Rolandi, R.; Morgante, A.; Floreano, L.; Canepa, M. *The Journal of Physical Chemistry B* **2005**, *109*, 18003-18009.
- (47) Zhang, W. W.; Lu, C. S.; Zou, Y.; Xie, J. L.; Ren, X. M.; Zhu, H. Z.; Meng, Q. J. *Journal of Colloid and Interface Science* **2002**, *249*, 301-306.
- (48) Naumkin, A. V.; Kraut-Vass, A.; Gaarenstroom, S. W.; Powell, C. J. *NIST X-ray Photoelectron Spectroscopy Database*.
- (49) Jana, S.; Srivastava, B. B.; Acharya, S.; Santra, P. K.; Jana, N. R.; Sarma, D. D.; Pradhan, N. *Chemical Communications* **2010**, *46*, 2853-2855.
- (50) Srivastava, B. B.; Jana, S.; Pradhan, N. *Journal of the American Chemical Society* **2010**, *133*, 1007-1015.
- (51) Gul, S.; Cooper, J. K.; Corrado, C.; Vollbrecht, B.; Bridges, F.; Guo, J.; Zhang, J. Z. *The Journal of Physical Chemistry C* **2011**, *115*, 20864-20875.
- (52) Brovelli, S.; Galland, C.; Viswanatha, R.; Klimov, V. I. *Nano Letters* **2012**, *12*, 4372-4379.
- (53) van Driel, A. F.; Allan, G.; Delerue, C.; Lodahl, P.; Vos, W. L.; Vanmaekelbergh, D. *Physical Review Letters* **2005**, *95*, 6804-6807.
- (54) de Mello Donegá, C.; Koole, R. *The Journal of Physical Chemistry C* **2009**, *113*, 6511-6520.
- (55) Hens, Z.; Moreels, I. *Journal of Materials Chemistry* **2012**, *22*, 10406-10415.
- (56) Merzbacher, E. *Quantum Mechanics, 2nd ed; Wiley International Edition: New York* **1970**.
- (57) Moreels, I.; Lambert, K.; Smeets, D.; De Muynck, D.; Nollet, T.; Martins, J. C.; Vanhaecke, F.; Vantomme, A.; Delerue, C.; Allan, G.; Hens, Z. *ACS Nano* **2009**, *3*, 3023-3030.
- (58) Karel Capek, R.; Moreels, I.; Lambert, K.; De Muynck, D.; Zhao, Q.; Van Tomme, A.; Vanhaecke, F.; Hens, Z. *The Journal of Physical Chemistry C* **2010**, *114*, 6371-6376.
- (59) Empedocles, S. A.; Norris, D. J.; Bawendi, M. G. *Physical Review Letters* **1996**, *77*, 3873-3876.
- (60) Moreels, I.; Rainò, G.; Gomes, R.; Hens, Z.; Stöferle, T.; Mahrt, R. F. *Acs Nano* **2011**, *5*, 8033-8039.
- (61) Choy, J. T.; Hausmann, B. J. M.; Babinec, T. M.; Bulu, I.; Khan, M.; Maletinsky, P.; Yacoby, A.; Loncar, M. *Nature Photonics* **2011**, *5*, 738-743.
- (62) Shirasaki, Y.; Supran, G. J.; Bawendi, M. G.; Bulovic, V. *Nature Photonics* **2013**, *7*, 13-23.

## FIGURES

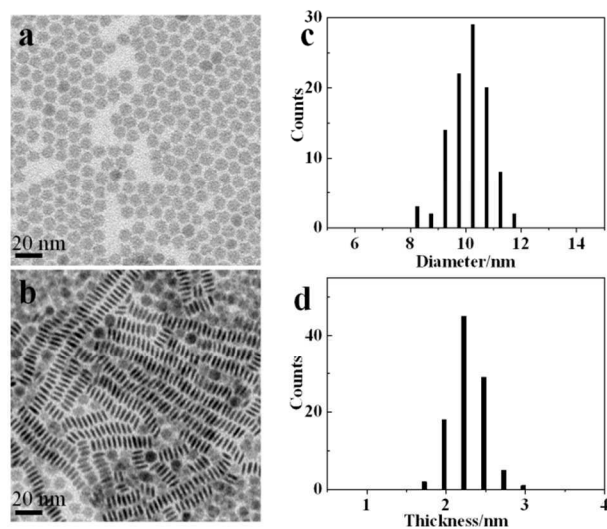


**Figure 1.** (a,b) BF-TEM images of copper telluride nanodisks. Nanodisk stacks allow determining their thickness. (c,d) Corresponding size histograms showing the diameter and thickness of the nanodisks. The histograms were constructed using a binning of 0.5 nm and 0.25 nm for the diameter and thickness respectively.

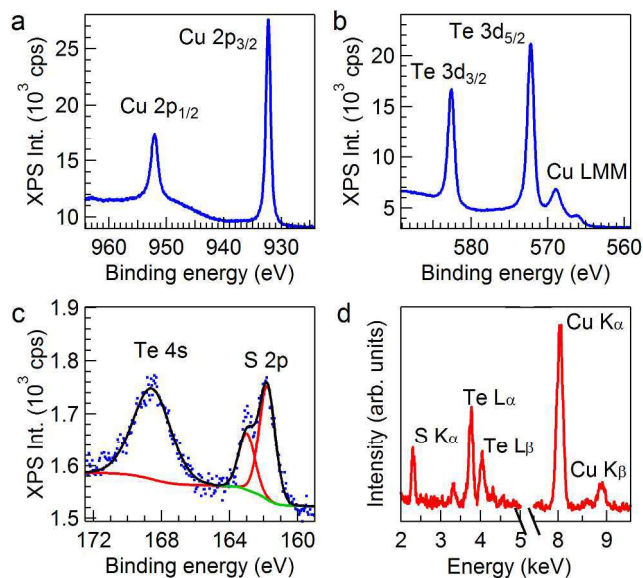


**Figure 2.** (a-c) XPS analysis on the copper telluride nanodisks: (a) Cu 2p doublet, (b) Te 3d doublet and Cu LMM Auger peak, (c) Te 4s and S 2p peaks, together with data fitting for quantitative comparison. Shirley-type background and voigt profiles were used in the procedure. S 2p doublet separation was set to 1.2 eV. (d) EDS overview spectrum, obtained on an area containing several Cu<sub>2</sub>Te nanodisks.

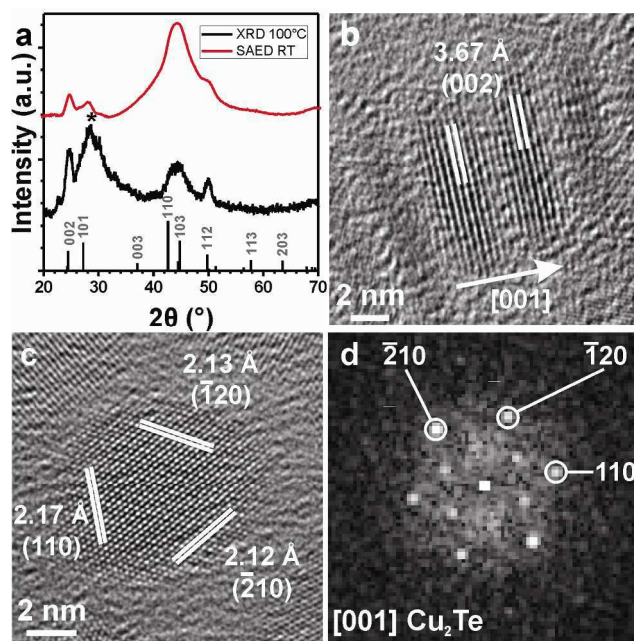


**Figure 3.** (a) XRD pattern collected on  $\text{Cu}_2\text{Te}$  nanodisks after a short annealing in vacuum at  $100^\circ\text{C}$ , compared to the radially integrated intensity profile from a SAED pattern acquired at room temperature from a region including several  $\text{Cu}_2\text{Te}$  nanodisks. Both patterns exhibit a good match with hexagonal  $\text{Cu}_2\text{Te}$  (space group  $P6/mmm$ , ICSD structure #77055). (\*) marks a broad reflection arising from the miscut silicon (111) substrate. (b-c) HRTEM images of: (b) disk stacks, showing the  $[001]$  direction of  $\text{Cu}_2\text{Te}$  oriented perpendicular to the surface for each nanodisk, and (c) a disk with the flat face parallel to the support film. (d) The fast Fourier transform (FFT) of (c) shows the  $[001]$  pattern of  $\text{Cu}_2\text{Te}$ , confirming that the  $c$ -axis is perpendicular to the flat face of the disks. The HRTEM images were frequency-filtered, in order to emphasize the crystalline features.

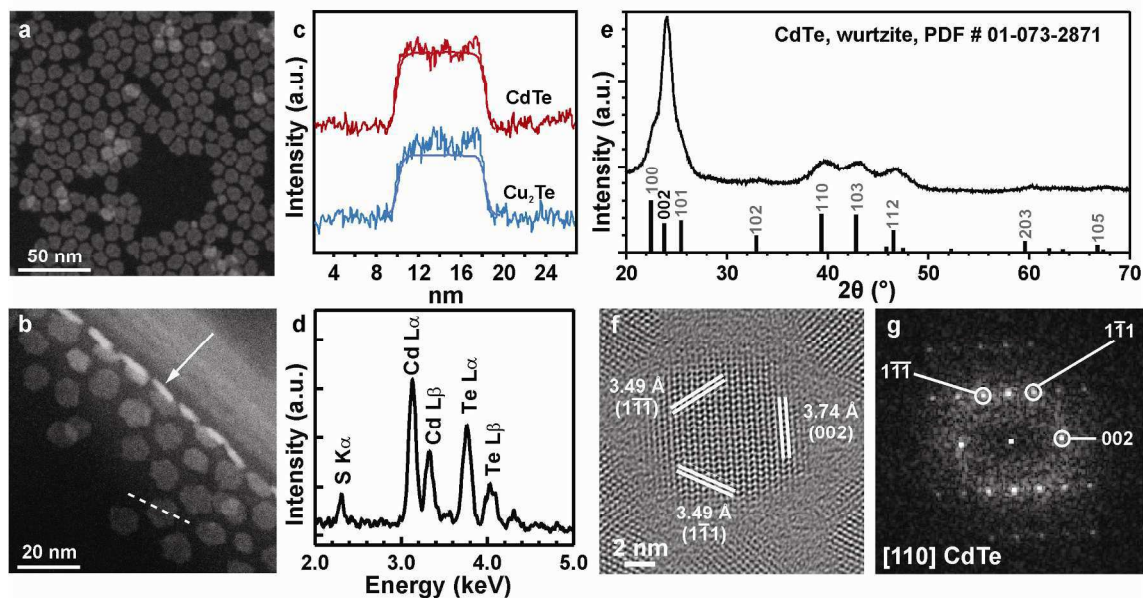


**Figure 4.** (a) HAADF-STEM overview image of the CdTe quantum disks. (b) Some disks (*e.g.*, the one pointed by the arrow) adhere vertically to the lacey carbon net edge, allowing unambiguous determination of their shape. (c) Comparison of the HAADF-STEM intensity profiles (typically along the direction as indicated in (b) by the dashed line) from a CdTe quantum disk and a Cu<sub>2</sub>Te nanodisk, together with their respective simulated profile, confirming the flat top and bottom surface of both systems. The simulation was convolved with a probe size of about 1 nm, to take into account the experimental resolution. (d) EDS spectrum acquired over several CdTe nanodisks, showing contributions from the Cd- and Te- core atoms, and S-atoms from the C<sub>12</sub>SH ligands. (e) XRD pattern, in agreement with wurtzite CdTe (space group P6<sub>3</sub>mc, JCPDS Card no. 01-0732871). (f) HRTEM image of a typical CdTe quantum disk, and (g) corresponding FFT demonstrating that the flat surface is parallel to a [110]-oriented plane of wurtzite CdTe.

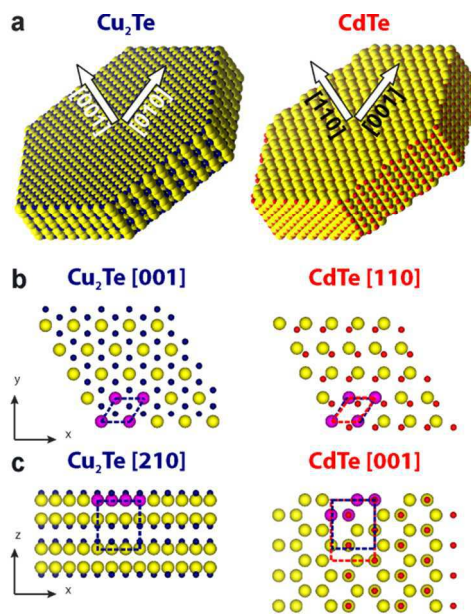


**Figure 5.** (a) Sketches of the Cu<sub>2</sub>Te and CdTe disks, with arrows indicating the respective crystal orientations. (b-c) Schematic views of slabs of the Cu<sub>2</sub>Te and CdTe structures, showing a few atomic layers of the nanodisks according to the respective phases and orientations determined by HRTEM. Each Te anion (larger yellow spheres) in the (001) plane of Cu<sub>2</sub>Te forms a hexagonal lattice (cell indicated by blue dashed lines) with the three neighboring anions (magenta) on the same plane. The (110) anionic sublattice in wurtzite CdTe still resembles a distorted hexagon in projection (red dashed lines). However, the Te atoms of the original Cu<sub>2</sub>Te structure have to move considerably in the *z*-direction to adapt the Cd atoms and form the two (110) layers in wurtzite CdTe. The volume occupied by the same number of Te atoms is included within the blue and red frames in Cu<sub>2</sub>Te and CdTe, respectively.

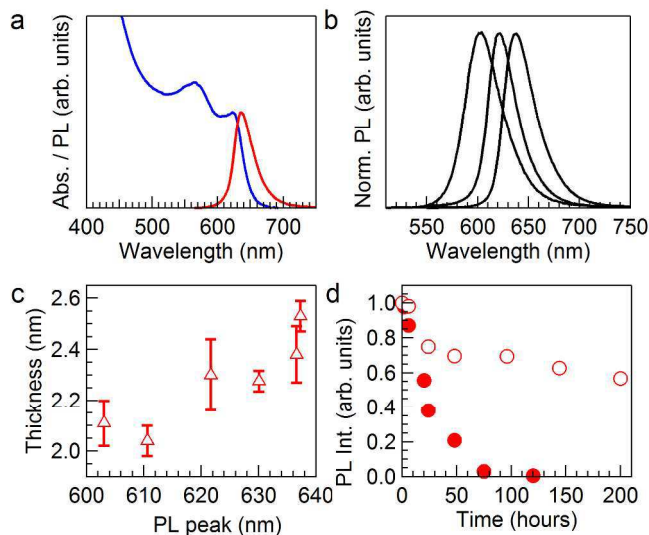


**Figure 6.** (a) Typical absorbance and PL spectrum, for 10 nm by 2.9 nm CdTe quantum disks.

(b) Series of PL spectra. (c) The PL peak position scales with the quantum disk thickness. The error on the average thickness is given as the 95% confidence interval, equal to  $1.96\sigma/\sqrt{N}$ , with  $\sigma$  the standard deviation and  $N$  the number of particles. (d) Optical stability under ambient conditions of CdTe quantum disks compared to spherical CdTe quantum dots obtained by a conventional approach. The PL intensity decreases more slowly with time for the disks.



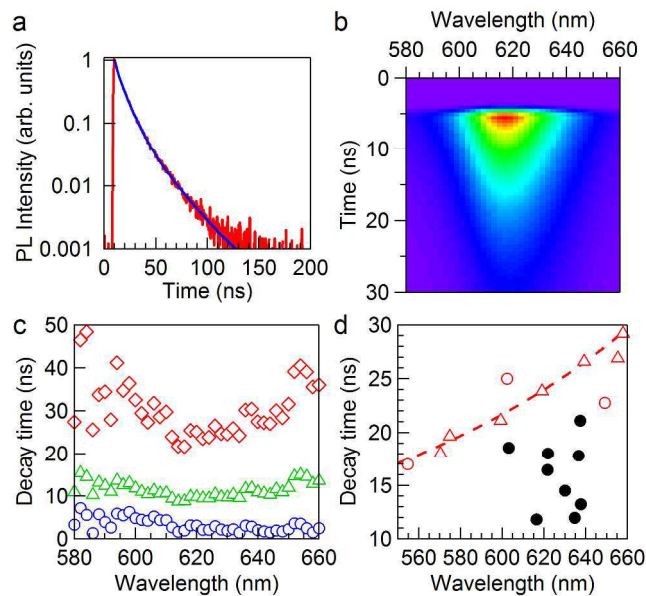


**Figure 7.** (a) Typical decay trace, for a sample with emission peak at 616 nm, with tri-exponential fit. (b) Spectral dependence of the decay. (c) Resulting decay components obtained from the fit. (d) Lifetime-weighted average decay time for quantum disks (full dots), spherical quantum dots (open circles) and literature data on dots (triangles). The quantum dot data agree with a fitted curve proposed in ref. 47, and the quantum disks show, on average, a 36% faster lifetime.



## TOC GRAPHIC (updated)

